A New Look at an Old Reaction: The Potential Energy Surface for the Thermal Carbonylation of $Mn(CO)_5CH_3$. The Role of Two Energetically Competitive Intermediates on the Reaction Surface, and Comments on the Photodecarbonylation of $Mn(CO)_5(COCH_3)$

Agnes Derecskei-Kovacs[†] and Dennis S. Marynick*

Contribution from the Department of Chemistry and Biochemistry, University of Texas at Arlington, Arlington, Texas 76019-0065

Received September 22, 1999. Revised Manuscript Received December 28, 1999

Abstract: A detailed theoretical study of the carbonyl insertion reaction $Mn(CO)_5CH_3 + CO \rightarrow Mn(CO)_5(COCH_3)$ is presented using gradient corrected density functional theory. As has been well-documented experimentally, this reaction proceeds through a two-step mechanism. In the first step, a stereochemically well-defined intermediate is formed via migration of the methyl group to a cis carbonyl. In the second step, the incoming nucleophile attacks the intermediate to form product. Two stable intermediates have been located on the potential energy surface. Both are formally $Mn(CO)_4(COCH_3)$; however, in one case the intermediate is stabilized by a strong agostic interaction between a methyl group hydrogen and the metal, and in the second case the acyl group distorts to form an Mn−O bond and thus acts as an η^2 (dihapto) ligand. The transition states between the reactant and the intermediates have been located. In addition, the transition states for CO attack of each intermediate have also been characterized. A detailed kinetic analysis of two possible reaction channels demonstrates that the solvent unassisted mechanism proceeds via CO attack on the agostic intermediate, even though the dihapto intermediate is lower in energy. Our calculated energetics (both activation energy and overall exothermicity) are in excellent agreement with experiment. We have also investigated some aspects of the photodecarbonylation of $Mn(CO)_5(COCH_3)$ to yield $Mn(CO)_5CH_3$. This reaction has been proposed to proceed via the dihapto intermediate, and we confirm this result on the basis of a comparison of calculated vs observed CO stretching frequencies of the experimentally characterized intermediate. Therefore, the thermal carbonylation of $Mn(CO)_5CH_3$ and the photodecarbonylation of $Mn(CO)_5(COCH_3)$ proceed along different reaction channels. Some additional comments on the role of solvent in the photodecarbonylation of $Mn(CO)_5(COCH_3)$ are included. Specifically, we find (again on the basis of a comparison of calculated vs experimentally observed vibrational frequencies) that the dihapto intermediate in the photodecarbonylation experiments is unsolvated, even in coordinating solvents such as THF.

Introduction

The alkyl group migration reaction is one of the most fundamental reactions in all of organometallic chemistry.[1−15] Perhaps the classic example of this general reaction, and one often discussed in textbooks,[16] is the carbonylation of pentacarbonyl(methyl)manganese(I), which is well-established to occur via a two-step process:

$$\underset{\mathbf{a}}{Mn(CO)_5CH_3} \leftrightarrows \mathbf{I} \xrightarrow{CO^*} \underset{\mathbf{b}}{Mn(CO)_4(CO)^*(COCH_3)} \quad (1)$$

While this reaction is often referred to as the "carbonyl insertion reaction", stereochemical evidence[5] has clearly demonstrated that the incoming nucleophile in the second step of this reaction appears cis to the newly formed acyl group, and therefore the process may be viewed as a migration of CH_3 to an adjacent CO resulting in an intermediate **I** (a formally coordinatively

[†] Present address: Department of Chemistry, Texas A&M University, College Station, TX 77843-3012.

(1) Kuhlmann, E. J.; Alexander, J. J. *Coord. Chem. Rev.* **1980**, *33*, 195. Wojciki, A. *Adv. Organomet. Chem*. **1973**, *11*, 87. Calderazzo, F. *Angew. Chem., Int. Ed. Engl*. **1977**, *16*, 299.

(2) (a) Mawby, R. J.; Basolo, F.; Pearson, R. G. *J. Am. Chem. Soc.* **1964**, *86*, 3994. (b) Wax, J. J.; Bergman, R. G.. *J. Am. Chem. Soc.* **1981**, *103*, 7028.

(3) Calderazzo F.; Cotton, F. A. *Inorg. Chem.* **1962**, *1*, 30.

(4) Noack, K.; Calderazzo, F *J. Organomet. Chem.* **1967**, *10*, 10.

(5) Flood, T. C.; Jensen, J. E.; Statler, J. A. *J. Am. Chem. Soc*. **1981**, *103*, 4410. Noack, K.; Calderazzo, F. *J. Organomet. Chem*. **1967**, *10*, 101. Cotfield, T. H.; Kozikowske, J.; Closson, R. N. *J. Org. Chem.* **1957**, *22*, 598. *Spec. Publ. Chem. Soc*. **1959**, *13*, 126.

(6) McHugh, T. M.; Rest, A. J. *J. Chem. Soc., Dalton Trans.* **1980**, 2323.

(7) Nickolas, K.; Raghu, S.; Rosenblum, M. *J. Organomet. Chem.* **1974**, *78*, 133.

(8) Mashima. K.; Nakamura, A. *J. Organomet. Chem.* **1992**, *428*, 49.

(9) Brookhart, M.; Green, M. L. H.; Wong, L. L. *Prog. Inorg. Chem.* **1988**, *36*, 1.

(10) Berke, H.; Hoffmann, R. *J. Am. Chem. Soc.* **1978**, *100*, 7224.

(11) Ziegler, T.; Versluis, L.; Tschinke, V. *J. Am. Chem. Soc.* **1986**, *108*, 612.

(12) Saddei, D.; Freund, H. J.; G. Holnecher, G. *J. Organomet. Chem.* **1980**, *186*, 63.

(13) Ruiz, M. E.; Flores-Riveros, A.; Novaro, O. *J. Catal. 1980*, *64*, 1.

(14) Axe, F. U.; Marynick, D. S. *Organometallics* **1987**, *6*, 572.

(15) Axe, F. U.; Marynick, D. S. *J. Am. Chem. Soc.* **1988**, *110*, 3728.

(16) See for instance: Cotton, F. A.; Wilkinson, G.; Murillo, C. A.; Bochmann, M. *Advanced Inorganic Chemistry*, 6th ed.; John Wiley & Sons: New York, 1999. Miessler, G. L.; Tarr, D. A. *Inorganic Chemistry*, 2nd ed.; Prentice Hall: Englewood Cliffs, NJ, 1998. Huheey, J. E.; Keiter, E. A.; Keiter, R. L. *Inorganic Chemistry*, 4th ed.; Harper Collins: New York, 1993. Douglas, B.; McDaniel, D.; Alexander, J. *Concepts and Models of Inorganic Chemistry*, 3rd ed.; John Wiley & Sons: New York, 1994.

10.1021/ja993441v CCC: $19.00
Published on Web 02/19/2000

unsaturated species), followed by addition of CO* to the "vacant" coordination site of **I**. This mechanism appears to apply to a wide variety of incoming nucleophiles **L**,[2a] for which the rates are first order in both $Mn(CO)_5CH_3$ and **L** at low nucleophile concentrations, but at high nucleophile concentrations the rate of the reaction becomes independent of **L**. Such behavior is easily reconcilable with the two-step mechanism shown in eq 1, assuming **I** is a steady-state intermediate. While there is substantial evidence for the existence of **I** as a stable intermediate on the methyl migration potential energy surface, the nature of the intermediate has been the subject of considerable speculation.[5−7,10−15] **I** could be envisioned as a coordinatively unsaturated acyl species (**c**), a coordinatively saturated species with an η^2-acyl group (**d**), or a coordinatively unsaturated species stabilized by an agostic interaction between a C−H hydrogen and the manganese (**e**). Species **c** would almost certainly be solvent stabilized to some extent, since a five-coordinate coordinatively unsaturated species such as this would be expected to be stereochemically nonrigid, and could not account for the exclusive cis stereochemistry found in the product.

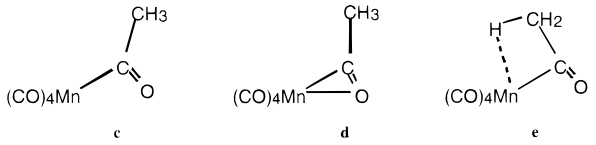

Polar solvents enhance the rate of reaction 1. This was originally interpreted as a dielectric effect, since the reaction rate shows a near linear dependence on the appropriate function of the dielectric constant of the solvent and the intermediate was thought to be more polar than the reactant.[3] However, it has also been proposed that coordinating solvents stabilize **c** by direct solvent coordination to the vacant binding site.[2] A troubling feature of this interpretation is that it is difficult to understand why direct coordination of solvent, which blocks the site destined for the incoming nucleophile, should enhance the rate of nucleophilic attack. A possible resolution of this difficulty comes from a detailed kinetic study of a closely related system *p*-$CH_3OC_6H_4CH_2Mn(CO)_5$, in which it was demonstrated that solvent does not enhance the rate by stabilizing the intermediate, but rather by catalyzing its formation.[17]

Recently, Boese, et al.[18,19] took a new approach to the study of this system, by examining the photo*decarbonylation* of **b** to form **a**. While the photodecarbonylation of **b** is not the precise microscopic reverse of reaction 1, the nature of the intermediates in this reaction may well be relevant to the mechanism of the carbonylation reaction. Boese et al. did indeed observe a long-lived transient in the decarbonylation reaction, the time-resolved infrared spectra of which exhibited only modest dependence on solvent. Based on kinetic and spectroscopic evidence they suggested that the form of the stable intermediate in weakly coordinating solvents is **d**, while in strongly coordinating solvents **c** (solvent-stabilized) predominates. They were not able to interpret the role of **e** in the reaction.

Only a limited number of theoretical studies have been published for this system. Extended Hückel calculations predicted that **d** was not a minimum on the potential energy surface.[10] However, more accurate local density functional[11] and PRDDO/ab initio calculations[14,15] predicted that **d** was very stable. The structure and stability of **e**, however, has never been investigated at any theoretical level. Given the recent experimental work which clearly points to **d** as an important intermediate in the photodecarbonylation of **b,** it is now appropriate to examine the geometries and relative energies of **a**, **d**, and **e** along with the possible activated complexes at a higher theoretical level.

In this paper, we present such a study, using gradient corrected density functional methods. We demonstrate that the unsolvated thermal carbonylation and photodecarbonylation processes move along different reaction channels on the potential energy surface. We show that although the η^2-stabilized species **d** is the stable intermediate for the photodecarbonylation reaction, the thermal carbonylation process proceeds through the agostically stabilized structure **e** as the intermediate. We also present the activated complexes for both the methyl migration and carbonyl insertion steps along with a discussion of reaction kinetics for the two reaction channels. Finally, we comment on the role of solvent stabilization of the transient found in the photodecarbonylation experiments.

Calculations

We performed full gradient optimization on all structures, using density functional theory (DFT) as implemented in the Gaussian 94 program[20] with the B3P86 functional. The performance of this gradient-corrected functional has been tested and found to be very good[21] in comparison with high level correlated ab initio results. Two different basis sets were used for the description of the metal atom and ligand system. The smaller basis set (**sb**) contained a polarized split valence representation of the Mn atom specifically developed for DFT calculations.[22,23] This basis set used the standard 6-31G** (5d) level of description for the ligands. The larger basis sets (**lb**) contained a triple-ζ representation of the metal atom and one f polarization function (Wachters + f[24−26]). For the description of the ligand system, the 6-311++G** (5d) basis set was employed. All geometry optimizations were performed in the all electron approximation using the smaller basis set and the B3P86 functional. All stationary points on the potential energy surface for reaction 1 were fully characterized by frequency calculations at this level. We also located two minima for species **c** with explicit solvent (THF) coordination at the vacant site, i.e., $Mn(THF)(CO)_4(COCH_3)$. To analyze the sensitivity of the potential energy

(17) Webb, S. L.; Giandomenico, C. M.; Halpern, J. *J. Am. Chem. Soc.* **1986**, *108*, 34.
(18) Boese, W. T.; Lee, B.; Ryba, D. W.; Belt, S. T.; Ford, P. C. *Organometallics* **1993**, *12*, 4739.
(19) Boese, W. T.; Ford, P. C. *J. Am. Chem. Soc.* **1995**, *117*, 8381.
(20) GAUSSIAN 94 (Revision D.4), Frisch, M. J.; Trucks, G. W.; Schlegel, H. B.; Gill, P. M. W.; Johnson, B. G.; Robb, M. A.; Cheeseman, J. R.; Keith, T.; Petersson, G. A.; Montgomery, J. A.; Raghavachari, K.; Al-Laham, M. A.; Zakrzewski, V. G.; Ortiz, J. V.; Foresman, J. B.; Cioslowski, J.; Stefanov, B. B.; Nanayakkara, A.; Challacombe, M.; Peng, C. Y.; Ayala, P. Y.; Chen, W.; Wong, M. W.; Andres, J. L.; Replogle, E. S.; Gomperts, R.; Martin, R. L.; Fox, D. J.; Binkley, J. S.; Defrees, D. J.; Baker, J.; Stewart, J. P.; Head-Gordon, M.; Gonzalez, C.; Pople, J. A. Gaussian, Inc.: Pittsburgh, PA, 1995.
(21) Johnson, B. G.; Gill, P. M. W.; Pople J. A. *J. Chem. Phys.* **1992**, *97*, 10. Gill, P. M. W.; Johnson, B. G. J. A. *Chem. Phys. Lett.* **1992**, *197*, 499. Johnson, B. G.; Gill, P. M. W.; Pople J. A. *J. Chem. Phys.* **1993**, *98*, 5612. Oliphant, N.; Bartlett, R. J. *J. Chem. Phys.* **1994**, *100*, 6550.
(22) Basis sets were obtained from the Extensible Computational Chemistry Environment Basis Set Database, Version 1.0, as developed and distributed by the Molecular Science Computing Facility, Environmental and Molecular Sciences Laboratory, which is part of the Pacific Northwest Laboratory, P.O. Box 999, Richland, WA 99352, USA, and funded by the U.S. Department of Energy. The Pacific Northwest Laboratory is a multiprogram laboratory operated by Battelle Memorial Institue for the U.S. Department of Energy under contract DE-AC06-76RLO 1830. Contact David Feller, Karen Schuchardt, or Don Jones for additional information.
(23) Godbout, N.; Salahub, D. R.; Anzhelm, J.; Wimmer, E. *Can. J. Chem.* **1992**, *70*, 560.
(24) Wachters, A. F. *J. Chem. Phys.* **1969**, *52*, 1033.
(25) Wachters, A. J. IBM Tech. Rept. RJ584, 1969.
(26) Bauschlicher, C. W., Jr.; Langhoff, S. R.; Barnes, L. A. *J. Chem. Phys.* **1989**, *91*, 2399.

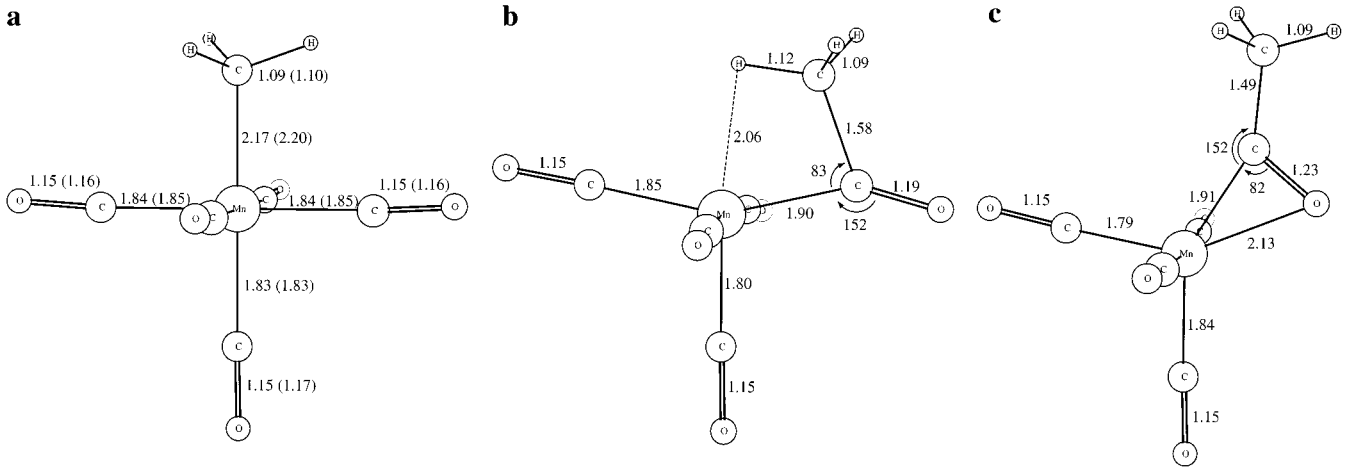

Figure 1. (a) Optimal geometry of the reactant (**a**). (b) Optimal geometry of the agostic form (**e**). **(**c) Optimal geometry of the dihapto form (**d**). Distances are in angstroms and angles in degrees. Experimental data are in parentheses. All optimized geometries are calculated at the B3B86/**sb** level.

surface to basis set and correlation effects, the relative energies were reevaluated using the larger basis, **lb**, and the B3P86 and B3LYP gradient corrected density functionals. Final energetics were taken from the B3LYP/**lb**//B3P86/**sb** calculations, since they gave the best overall agreement with the experimentally known $\Delta H°$ for reaction 1 (see below). For some species, we also did single-point calculations at the QCISD level using theB3P86/**sb** geometries with the **sb** basis set. Calculations were performed on IBM RS6000 workstations (Models 370 and 595) as well as SGI Origin 2000 and NEC SX4 computers.

Results

First Step in the Carbonylation of $Mn(CO)_5CH_3$: Methyl Migration. Figures 1 presents the fully optimized geometries for three minima on the $Mn(CO)_5CH_3$ potential energy surface.[27]Only the reactant has been characterized structurally.[29] As can be seen in Figure 1a, B3P86/**sb** calculations yielded metal−ligand distances in very good agreement with experiment. Figure 1b demonstrates that the structure of the agostic form is somewhat unusual. The Mn−C−C angle in the acyl group is only 83° while the Mn−C−O angle is 152°. Clear evidence of an agostic interaction is present. The agostically bound hydrogen has a C−H distance of 1.12 Å, while the Mn−H distance is 2.06 Å. Attempts to locate a true coordinatively unsaturated five-coordinate intermediate with a "normal" acyl geometry (bond angles ca. 120°) failed: these structures inevitably collapsed to the agostic species or the dihapto form. To validate the assumption that an agostic H−Mn interaction is responsible for this distortion of the geometry, we rotated the methyl group by 60°, artificially disengaging the agostic interaction. After reoptimizing the hydrogen positions at a lower theoretical level, we obtained an energy 10.9 kcal/mol higher than **e**. This yields a rough estimate of the strength of the agostic interaction. We then allowed the system to relax completely, and it smoothly collapsed into the reactant. Consequently, the agostic interaction must be the main factor stabilizing **e**. In fact, the traditional acyl form is not a minimum on the potential energy surface but (as is shown later) a transition state. Figure 1c illustrates that the dihapto form also has a distorted geometry when compared to the traditional acyl conformation. The distortion compresses the Mn−C−O angle from 120° to 82° and increases the Mn−C−C angle to 152°.

To calculate the activation energy for methyl migration in $Mn(CO)_5CH_3$, the transition states between the reactant and the agostic forms (**ts1**) and between the agostic and the dihapto forms (**ts2**) were fully optimized. Panels a and b in Figure 2 depict the optimized geometries for the two transition states. Structure **ts1** exhibits the same unusual small angle acyl conformation as **e** and it is somewhat stabilized by the agostic interaction. Remarkably, **ts1** is only 0.1 kcal/mol less stable than **e** at the B3LYP/**lb** level. Despite this small back-reaction barrier, **ts1** is a well-defined transition state, with one imaginary frequency of 290*i* cm^{-1}. It is likely that the stability of **ts1** is somewhat overestimated by DFT. QCISD calculations (see below) place **ts1** 2.0 kcal/mol higher in energy than **e**. In **ts2**, the Mn−O bond has already started to form and the formation of the C−C bond in the acyl group is almost complete. An interesting aspect of **ts2** is that the methyl group has rotated 60° from the agostic form, with the in-plane hydrogen now pointing away from the metal. The expected structure, in which the in-plane hydrogen points toward the metal, is a second-order saddle point that optimized to **ts2** when the structure was distorted along the appropriate imaginary vibrational mode. This structure is the only extremum found in this region of the potential energy surface that has an η^1 bonding mode for the acyl group.

Why is **ts2** a transition state, rather than a true minimum? A simple explanation is offered by the nature of the LUMO (Figure 3a). This orbital, which is highly localized on Mn and dominantly of d character, is clearly well-positioned to accept an electron pair from either the methyl or the carbonyl side. The relevant occupied orbital is the HOMO (Figure 3b), which has both significant carbonyl in-plane lone pair character and acyl C−C character. Changing the Mn−C−O angle results in mixing of these two orbitals and collapse of the acyl group toward either the reactant or the dihapto species.

Table 1 presents the relative energies for all five species relevant to the first step of the reaction as calculated at various levels. To compare the DFT energetics with those of traditional

(27) We also attempted to optimize the molecules at the HF and MP2 levels using the same basis set. The reactant and the dihapto form were minima on the potential energy surface but the agostic form smoothly collapsed to the reactant. Overall, DFT appeared to give more reasonable geometries, which was not unexpected for a first row transition metal complex. The HF and MP2 relative energies were also unsatisfactory, in accordance with the observation of Niu and Hall,[29] who showed that the perturbation series for the migratory insertion step fails to converge in some systems. Therefore, we restricted our further geometry optimizations to gradient corrected density functionals.

(28) Niu, S.; Hall, M. B. *J. Phys. Chem.* **1997**, *A101*, 1360. Niu, S.; Hall, M. B. *J. Am. Chem. Soc.* **1997**, *119*, 3077.

(29) Seip, H. M.; Seip, R. *Acta Chem. Scand.* **1970**, *24*, 3431.

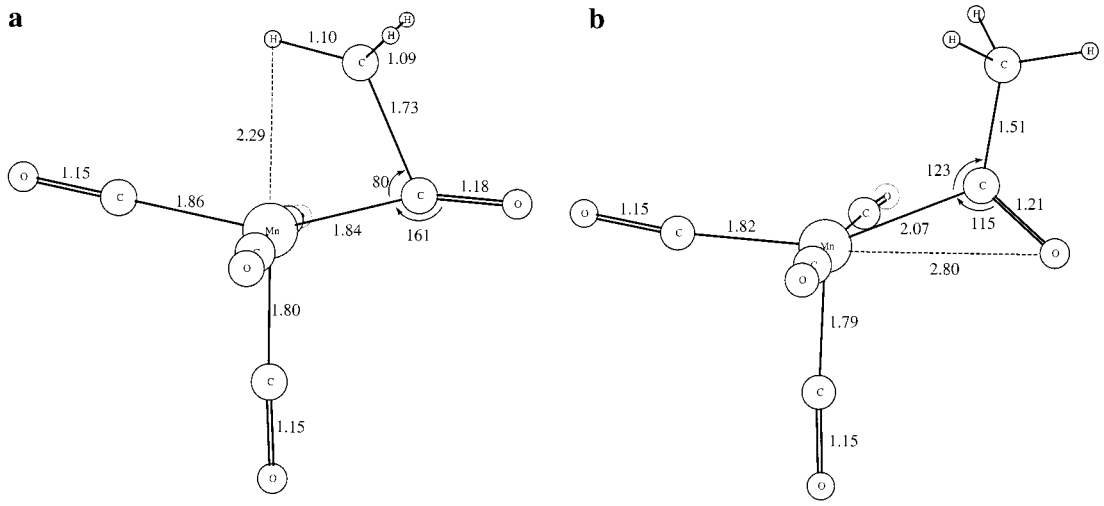

Figure 2. (a) Optimal geometry of the first transition state along the first reaction channel (**ts1**) in the methyl migration step. (b) Optimal geometry of the second transition state along the second reaction channel (**ts2**) in the methyl migration step. Distances are in angstroms and angles in degrees. All optimized geometries are calculated at the B3B86/**sb** level.

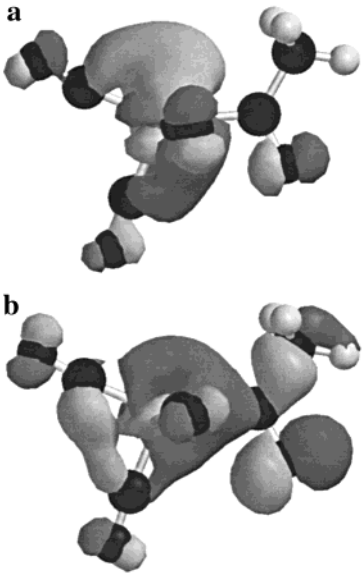

Figure 3. (a) Lowest unoccupied molecular orbital of **ts2**. (b) Second highest occupied molecular orbital of **ts2**. These plots were obtained with Spartan 5.0 using the SVWN functional and a double numerical plus polarization basis set.

Table 1. Relative Energies (in kcal/mol) of the Species Relevant First Step of the Carbonylation of $Mn(CO)_5(COCH_3)$ As Calculated with Different Methods at the B3P86/sb Optimal Geometry[a]

	structure	B3P86/**sb**	B3P86/**lb**	B3LYP/**lb**
reactant	**a**	0.0	0.0	0.0
trans. state	**ts1**	13.2	12.9	14.5
agostic	**e**	13.1	12.5	14.4
trans. state	**ts2**	25.7	25.1	23.1
dihapto	**d**	4.4	5.3	5.5

[a] Zero-point energy corrections calculated at the B3P86/sbll (scaled by 0.94) are included.

correlated ab initio methods, we performed single-point calculations on these structures at the QCISD/**sb** level, and found relative energies (kcal/mol) as follows: 0.0 (reactant), 15.6 (**ts1**), 13.6 (agostic form **e**), 33.4 (**ts2**), and 3.6 (dihapto form **d**). Except for **ts2**, which is calculated to be much less stable at the QCISD level, the QCISD results agree very well with those obtained from DFT. Given the excellent agreement between the two different density functionals and the large correlation correction calculated for **ts2** (the relative energy of **ts2** at the Hartree−Fock is only 18.0 kcal/mol, implying a correlation correction of over 15 kcal/mol), we believe that the DFT results are probably more reliable. As we shall see, our ultimate conclusions will not be affected by this discrepancy.

At all levels, the dihapto form is more stable than the agostic form. Also, all methods predict that the transition state between the agostic and the dihapto forms is higher in energy than the transition state between the reactant and the agostic form. Basis set effects did not appear to modify the relative energetic significantly in the DFT approximation.

Second Step in the Carbonylation of $Mn(CO)_5CH_3$: Carbonyl Insertion. According to the energetics described above, there are two possible reaction channels for the nonsolvent assisted carbonyl insertion reaction. Along channel 1 the reactant proceeds to the agostic form, which is attacked by the incoming CO. A second possibility (channel 2) is that the reactant proceeds to the agostic form and then to the more stable dihapto form, which is then attacked by CO. Both channels yield the same overall product, **b**. In both cases, the carbonyl insertion may occur either from the side of the acyl carbon atom or from the side of the acyl oxygen.

Let us consider channel 1 first. The two transition states for the carbonyl insertion into **e** are presented in panels a and b of Figure 4. Structure **ts3** (Figure 4a) shows the CO attack from the oxygen side and structure **ts4** (Figure 4b) that from the carbon side. Both transition states are distorted somewhat from the C_s symmetry (the O−C−Mn−acyl C dihedral angles are 3° and 17° in **ts3** and **ts4**, respectively). The O−C−Mn angle is not yet the 180° of a fully formed Mn−C bond but somewhat smaller (161°or 149°) with the carbonyl C located at 3.5 or 3.2 Å from the Mn atom. The agostic interaction is significantly weakened in both structures, and the Mn−H distance is elongated to 2.8 or 2.6 Å. The acyl groups in these transition states are arranged in conformations much closer to the traditional 120° than in **e** (the 152° angle of the O−C−Mn bond of **e** is reduced to 130° or 135°). CO attack on the agostic form is more likely to proceed through the formation of **ts4** (attack from the carbon side) since it has a lower activation energy than **ts3** (attack from the oxygen side) at all levels of theory.

For channel 2, the search for the transition state of the carbonyl attack from the carbon side was unsuccessful. Repeated attempts resulted in either nonconvergence or dissociation of

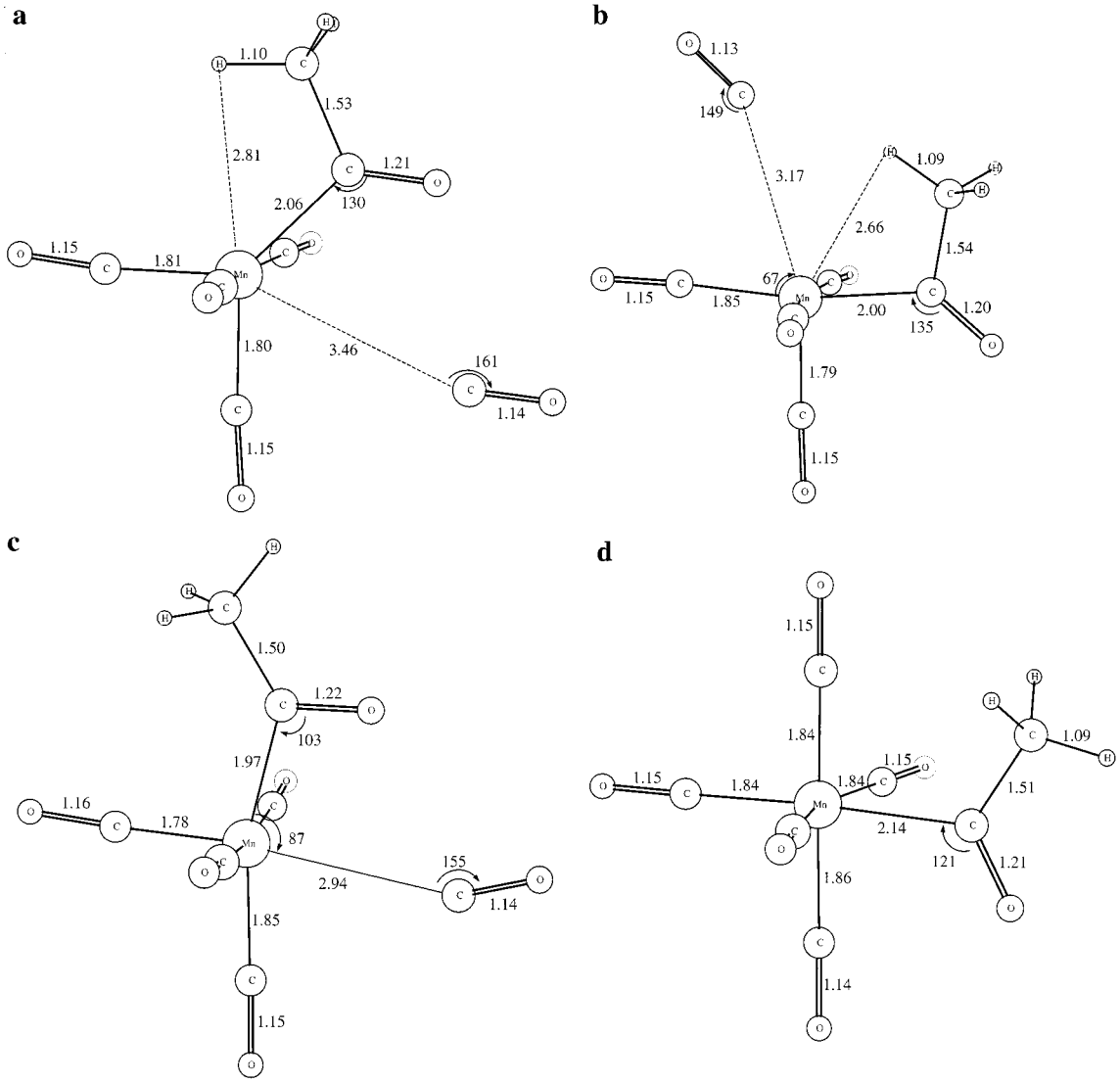

Figure 4. (a) Optimal geometry of one of the second transition states along the first reaction channel (**ts3**) in the carbonyl insertion step. (b) Optimal geometry of the other transition state along the first reaction channel (**ts4**) in the carbonyl insertion step. (c) Optimal geometry of the third transition state along the second reaction channel (**ts5**) in the carbonyl insertion step. (d) Optimal geometry of the overall product (**b**) of the carbonylation of $Mn(CO)_5CH_3$. Distances are in angstroms and angles in degrees. All optimized geometries are calculated at the B3B86/**sb** level.

Table 2. Relative Energies (in kcal/mol) of Species Relevant to the Second Step (carbonyl insertion) for the Carbonylation of $Mn(CO)_5(COCH_3)$ As Calculated with Different Methods at the B3P86/sb Optimal Geometry[a]

	structure	B3P86/**sb**	B3P86/**lb**	B3LYP/**lb**
trans. state	**ts3**	25.0	25.7	24.7
trans. state	**ts4**	18.6	19.3	19.8
trans. state	**ts5**	9.2	11.1	11.7
product	**b**	−17.0	−14.2	−8.8

[a]Zero-point energy corrections calculated at the B3P86/sb level (scaled by 0.94) are included.

the system to **d** + CO. The transition state for the attack from the oxygen side (**ts5**) can be seen in Figure 4c. This structure has almost perfect C_s symmetry (the O−C−Mn−acyl C dihedral angle is less than 1°) and the carbonyl group is found closer to the Mn atom than in **ts3** or **ts4** (2.9 Å). The Mn−acyl O bond is significantly weakened, the internuclear distance is 2.5 Å, and the acyl O−acyl C−Mn angle is less distorted from the traditional conformation (103°) than it was in **d**.

The energies of transition states **ts3**, **ts4**, and **ts5** and the overall product **b** (Figure 4d), relative to the sum of the energy of the free reactant and carbon monoxide, are listed in Table 2. Among the three transition states, **ts5** is the one with the lowest energy (the transition state for the last step along the second reaction channel). However, any conclusion about the availability of the two possible channels must be based on the analysis of the complete potential energy surface of the two-step mechanism and not on the relative stability of transition states in the individual steps. In addition, the absolute accuracy of the calculated potential energy surface must be validated. Let us first consider the details of the reaction kinetics.

Reaction Kinetics. For a more complete analysis of the kinetics of the thermal carbonylation process, one must analyze the kinetics along two reaction channels. The first channel involves formation of the agostic intermediate **e** and subsequent attack of CO. The second channel involves CO attack on the dihapto form **d**. The potential energy surfaces as calculated at the B3LYP/**lb** level are presented in Figures 5a (channel 1) and 5b (channel 2). The channel 1 mechanism:

$$\mathbf{a} \underset{k_{-1}}{\overset{k_1}{\rightleftharpoons}} \mathbf{e} \tag{2}$$

$$\mathbf{e} + \mathrm{CO} \underset{k_{-2}}{\overset{k_2}{\rightleftharpoons}} \mathbf{b} \tag{3}$$

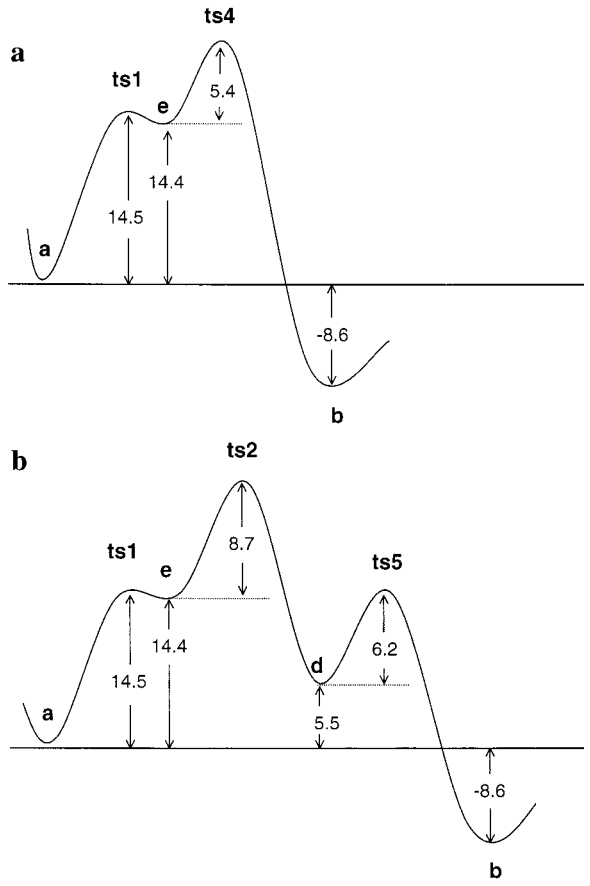

Figure 5. (a) B3LYP/**lb** potential energy surface for channel 1 of the thermal carbonylation of $Mn(CO)_5(COCH_3)$. (b) B3LYP/**lb** potential energy surface for channel 2 of the thermal carbonylation of $Mn(CO)_5(COCH_3)$ (energies in kcal/mol).

yields following rate equations

$$\frac{d[\mathbf{e}]}{dt} = k_1[\mathbf{a}] - k_{-1}[\mathbf{e}] - k_2[\mathbf{e}][CO] \tag{4}$$

$$\frac{d[\mathbf{b}]}{dt} = k_2[\mathbf{e}][CO] - k_{-2}[\mathbf{b}] \tag{5}$$

The steady-state approximation on the agostic intermediate **e** results in the following general rate equation:

$$\frac{d[\mathbf{b}]}{dt} = k_2[CO]\frac{k_1[\mathbf{a}] - k_{-2}[\mathbf{b}]}{k_{-1} + k_2[CO]} - k_{-2}[\mathbf{b}] \tag{6}$$

Since the activation energy of the reverse reaction is high (>23 kcal at the B3LYP/**lb**) we can assume that k_{-2} is small, and use a simplified rate equation:

$$\frac{d[\mathbf{b}]}{dt} = \frac{k_1}{\frac{k_{-1}}{k_2} + [CO]}[\mathbf{a}][CO] \tag{7}$$

On the basis of the Arrhenius equation $k = Ae^{-E_a/RT}$, one can estimate the k_{-1}/k_2 ratio if estimates of the relative preexponential factors can be made, e.g., if the ratio A_{-1}/A_2 can be approximated. In the calculations to follow, this ratio was estimated at 10^2 mol mL^{-1}. This estimate is based on a range of gas-phase unimolecular and bimolecular reactions, and the values may be rationalized on the basis of frequencies for simple bond stretches and collision frequencies.[30]

Assuming that the reaction proceeds via the agostic form (first channel), the k_{-1}/k_2 ratio turns out to be 8×10^5 at room temperature when using the B3LYP/**lb** activation energies of $E_1 = 0.1$ kcal/mol and $E_2 = 5.5$ kcal/mol. The experimental CO concentrations were obviously much smaller than this (their range can be estimated as $(1.5-5.0) \times 10^{-6}$ mol CO/mL of solvent based on the Bunsen coefficients[3]). Consequently, the rate expression for the two-step mechanism can be further simplified:

$$\frac{d[\mathbf{b}]}{dt} = \frac{k_1k_2}{k_{-1}}[\mathbf{a}][CO] \tag{8}$$

The reaction is first-order in both the reactant and CO, in full accordance with the experimental observations.[3] The effective activation energy of the overall reaction can be estimated as $E_{eff} = E_1 - E_{-1} + E_2 = 19.8$ kcal/mol. As we will see below, this value is very close to the experimental value extrapolated to a solvent with a dielectric constant of 1.[31]

The second reaction channel proceeds via the dihapto form **d**, which we will assume is formed from the agostic intermediate **e**.[32] The full reaction mechanism is:

$$\mathbf{a} \underset{k_{-1}}{\overset{k_1}{\rightleftharpoons}} \mathbf{e} \tag{9}$$

$$\mathbf{e} \underset{k_{-2}}{\overset{k_2}{\rightleftharpoons}} \mathbf{d} \tag{10}$$

$$\mathbf{d} + CO \underset{k_{-3}}{\overset{k_3}{\rightleftharpoons}} \mathbf{b} \tag{11}$$

Applying the steady-state approximation to **e** and **d** and again assuming $k_{-3} = 0$ yields:

$$\frac{d[\mathbf{b}]}{dt} = \frac{\frac{k_1k_2}{k_2 + k_{-1}}[\mathbf{a}][CO]}{[CO] + \frac{k_{-1}k_{-2}}{k_3(k_2 + k_{-1})}} \tag{12}$$

This equation can be further simplified by noting that $k_{-1} \gg k_2$, and

$$\frac{d[\mathbf{b}]}{dt} \approx \frac{\frac{k_1k_2}{k_{-1}}[\mathbf{a}][CO]}{[CO] + \frac{k_{-2}}{k_3}} \tag{13}$$

For the second channel, the k_{-2}/k_3 ratio turns out to be 4×10^{-7} at room temperature, which is about an order of magnitude *less* than the CO concentration. Therefore, one would not expect

(30) DeMore, W. B.; Sander, S. P.; Howard, C. J.; Ravinsshankara, A. R.; Golden, D. M.; Kolb, C. E.; Hampson, R. F.; Kurylo, M. J.; Molina, M. J. Chemical Kinetics and Photochemical Data for Use in Stratospheric Modeling, Evaluation No. 12, Jet Propulsion Laboratory, 1997.

(31) It should be noted that, if the DFT energetics are correct and **ts1** is only 0.1 kcal/mol less stable than **e**, then applying the steady-state approximation to **e** would probably not be valid at room temperature. In this case, the reaction is best thought of as being concerted and the calculated activation energy is 19.8 kcal/mol. However, as noted earlier, we think it is more likely that DFT is underestimating this energy difference and that **e** is a true intermediate.

(32) It is also possible that the agostic form **e** is not involved in the migration step at all. We could envision a third channel, in which **ts2** is the transition state between the reactant and the dihapto species, which is then attacked by CO. A detailed kinetic analysis of this third channel leads to conclusions essentially identical with those for channel 2.

the simple bimolecular rate dependence found experimentally. If our estimate of k_{-2}/k_3 is correct, then eq 14 reduces to

$$\frac{d[\mathbf{b}]}{dt} \approx \frac{k_1 k_2}{k_{-1}}[\mathbf{a}] \tag{14}$$

and the rate equation has the incorrect functional form. Of course, even assuming the calculated energetics are correct, our "back of the envelope" calculation may not have yielded the correct value for k_{-2}/k_3 because of the assumptions concerning the relative magnitude of the preexponential terms for uni- and bimolecular reactions. If in fact $k_{-2}/k_3 \gg [CO]$, eq 14 reduces to

$$\frac{d[\mathbf{b}]}{dt} \approx \frac{k_1 k_2 k_3}{k_{-1} k_{-2}}[\mathbf{a}][CO] \tag{15}$$

restoring the correct functional form of the rate expression. In this case, however, the observed activation energy is $E_{a1} + E_{a2} + E_{a3} - E_{a-1} - E_{a-2} = 11.1$ kcal/mol. As we shall see, this value is much lower than the experimental value extrapolated to a solvent with a dielectric constant of 1.[33]

In the next section of this paper we validate the accuracy of the calculated potential energy surface against experimental data.

The Accuracy of the Calculated Potential Energy Surface. The exothermicity of the overall carbonylation reaction was also measured in ref 3, and was found to be -12.7 kcal/mol in β,β'-dioxydiethyl ether. Fortunately, gas-phase heats of formation are available for $Mn(CO)_5CH_3$ and $Mn(CO)_5(COCH_3)$,[34] allowing the direct evaluation of $\Delta H°$ for this reaction. The experimental value in the gas phase is -8.0 ± 1.4 kcal/mol. After vibrational and thermal correction are applied to the B3LYP/lb energy difference, our calculated enthalpy of reaction is -9.0 kcal/mol, in essentially perfect agreement with experiment. It is for this reason that we have based the kinetic analysis above on the B3LYP/lb energetics.

Calderazzo and Cotton[3] also performed a detailed study of the dependence of the measured rates of the thermal carbonylation of $Mn(CO)_5CH_3$ on the dielectric constant of the solvent.[35] A good linear dependence was found between the logarithm of the rate constant and an appropriately chosen function of the dielectric constant. The experimental data of ref 3 are plotted in Figure 6 along with a linear least-squares fit. For our purposes, the linear fit was extrapolated to the unit value of the dielectric constant to estimate the activation energy in a vacuum. The extrapolated rate constant ($\log(k) = -4.99 \pm 0.29$) was used to determine the extrapolated activation energy in a vacuum under the assumption that the preexponential factor is relatively unchanged by solvent. We used the experimental values for the activation energy (14.8 kcal/mol) and rate constant at room temperature (8.99×10^{-3} L mol^{-1} s^{-1}) in β,β'-diethoxydiethyl ether in this calculation and obtained an extrapolated activation energy of 18.9 ± 0.4 kcal/mol. Our effective activation energy for channel 1, $E_{eff} = 19.8$ kcal/mol (at the B3LYP/**lb** level), agrees extremely well with this value.

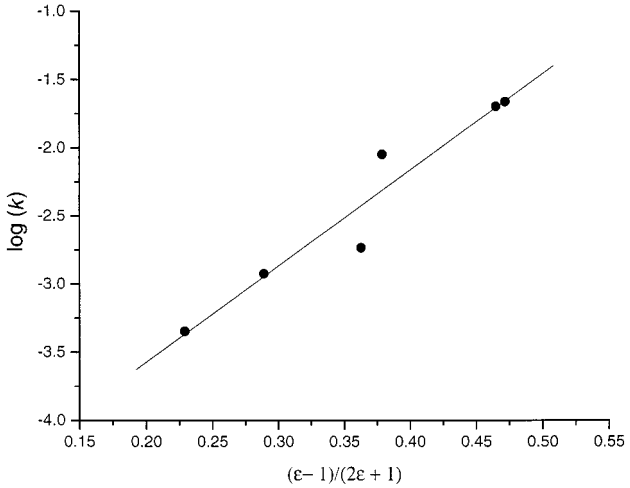

Figure 6. The experimental rate constant versus the dielectric constant of solvent at room temperature for the thermal carbonylation of $Mn(CO)_5(COCH_3)$. Data are taken from ref 3.

Photodecarbonylation of $Mn(CO)_5(COCH_3)$. During the photodecarbonylation of **b**, a long-lived intermediate was observed.[18,19] It was found experimentally that the rate of methyl migration does not exhibit a strong isotope effect upon changing the CH_3 group to CD_3, as one might expect for an agostically stabilized intermediate. Also, CF_3 and CH_2F substituted derivatives showed similar behavior; therefore, it was concluded that not the agostic form **e** but the dihapto stabilized structure **d** is the stable intermediate during photodecarbonylation. While our calculations are *not* consistent with the conclusion that **d** is an important intermediate in the carbonylation reaction, we show here the previous identification of **d** as the intermediate in the decarbonylation reaction *is* consistent with our calculations. However, we also provide evidence that, contrary to the interpretation of Boese et al.,[19] **d** is not explicitly solvent stabilize even in coordinating solvents such as THF.

First, we shall analyze the photodecarbonylation as it occurs in time. Under the effect of the incoming photon, a CO ligand is almost instantaneously removed from the overall product **b**, leaving behind an unstable system with an unoccupied coordination site. Then, this structure relaxes to eventually form **a**, the reactant of the carbonylation reaction. To model this process theoretically, we removed one CO unit from the fully optimized overall product and allowed the molecules to relax into an optimal geometry. While a rigorous treatment of this problem would require a molecular dynamics simulation (a computationally intractable option), this procedure should give us a qualitative feel for how close the initial product of the photodecarbonylation process is to the important stationary points on the reaction surface (**a**, **d**, and **e**). There are four symmetry unique positions (5 possible sites) where CO can be removed.[36] One of the structures, derived by removing an in-plane carbonyl cis to the acyl group and adjacent to the methyl group, optimized directly to the reactant **a**. One structure, derived by removing the carbonyl trans to the acyl group, optimized to a new minimum (of high energy) on the potential energy surface. The transition state between this minimum and the dihapto form was located, and the activation energy was found to be only

(33) It should be noted that if in fact the QCISD energetics more accurately reflect the relative energies of the stationary points, then the dihapto structure is completely inaccessible from the reactant side due to the very high energy of **ts2** at this level. In fact, the B3LYP/**lb** energetics which we have chosen to use in our kinetic and thermodynamic analyses yield the lowest relative energy for **ts2** and therefore represent a best-case scenario for the channel 2 mechanism.

(34) Connor, J. A.; Zafarani-Moattar, M. T.; Bickerton, J.; El Saied, N. I.; Suradi, S.; Carson, R.; Al Takhin; Skinner, H. A. *Organometallics* **1982**, *1*, 1166.

(35) As alluded to earlier, Calderazzo and Cotton assumed that the solvent effects observed were mainly a function of the bulk dielectric constant stabilizing a polar transition state and not specific solvent participation. In fact, the calculated dipole moments of all of the transition states and intermediates are considerably higher than that of the reactant. From the B3P86/**sb** calculations, we find the following (in Debye): **a** (0.3), **e** (3.0), **d** (3.0), **ts1** (2.4), **ts2** (2.7) **ts3** (2.1), **ts4** (3.8), and **ts5** (1.0).

(36) It is thought that photodissociation of **b** occurs only for carbonyls cis to the acyl group (ref 19).

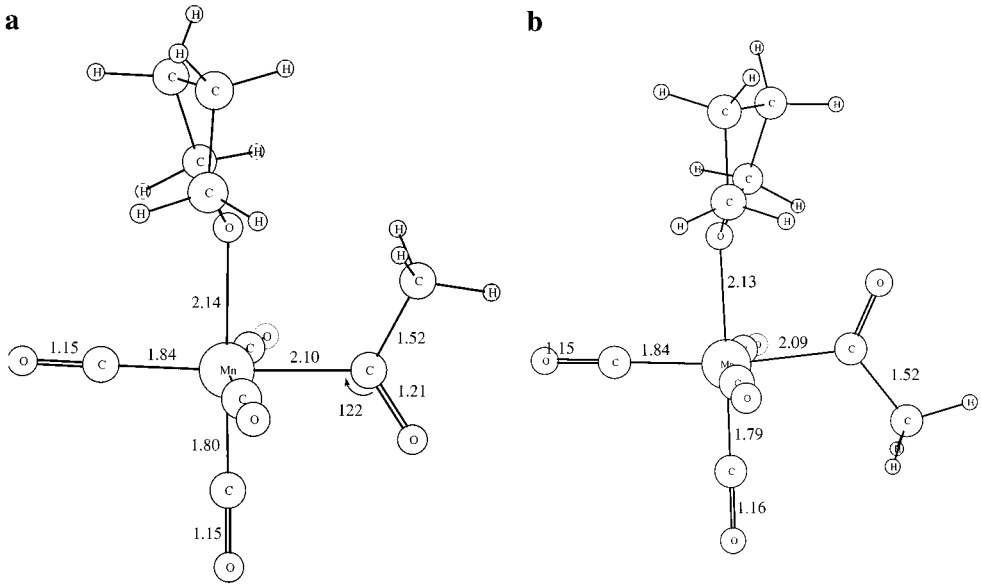

Figure 7. Two conformations of $Mn(THF)(CO)_4(COCH_3)$ optimized at the B3P86/**sb** level. Structure **f** (a) is 5.2 kcal/mol less stable than structure **g** (b) at the B3LYP/**lb** level.

Table 3. Calculated (B3P86/sb, see text) and Measured[18,19] Frequencies (in Hz) of the CO Stretches in the Intermediate of Photodecarbonylation of $Mn(CO)_5(COCH_3)$ (IR intensities in parentheses)

exptl[a]	**1607** (w)	1941[b]	1988 (s)	2080 (w)
exptl[c]	**1602** (w)	1928[b]	1977 (s)	2077 (w)
calcd for **d**[d]	**1609** (129)	1958 (908)	1978 (1490), 1986 (476)	2048 (211)
calcd for **e**[e]	**1784** (741)	1972 (953)	1983 (1452), 1988 (351)	2053 (172)
calcd for **f**[f]	**1661** (358)	1949 (722), 1953 (1385)	1969 (572)	2031 (247)
calcd for **g**[g]	**1677** (309)	1949 (1350), 1951 (857)	1971 (420)	2031 (314)

[a] Solvent is methylcyclohexane. [b] Experimental intensities were not given for the bands at 1941 and 1928 cm^{-1}; however, visual inspection of the published spectra[18,19] in cyclohexane indicate an intensity of about half that of the band labeled (s). [c] Solvent is THF. [d] Dihapto species. All calculated frequencies in this table are scaled by a factor of 0.94. [e] Agostic species. [f] $Mn(THF)(CO)_4(COCH_3)$, most stable conformation. [g] **g** is less stable than **f** by 3.0 kcal/mol at the B3P86/**sb** level.

1.3 kcal/mol at the B3P86/**sb** level. We were not able to identify a transition state yielding the reactant directly. The other three sites all smoothly relaxed to the dihapto form. Consequently, the removal of four CO units out of the possible five resulted in the formation of the dihapto form, the long-lived intermediate found experimentally during photodecarbonylation. The rearrangement of the dihapto form into the reactant requires a large amount of energy (approximately 18 kcal/mol at theB3LYP/**lb** level), which explains the high stability of the observed intermediate in the decarbonylation process.

A more direct comparison with experiment can be made by examining calculated vibrational frequencies of **e**, **d**, and two conformations of species **c** solvated with THF (species **f** and **g**, Figure 7), and comparing to experimental data at 195 K. Table 3 contains the B3P86 calculated frequencies (using a scaling factor of 0.94 and the **sb** basis set) in a vacuum and the measured CO stretch frequencies[18,19] in methylcyclohexane and THF.

The highest four calculated stretching frequencies belong to the carbonyl groups and they are relatively unaffected by the binding mode of the acyl group. The lowest frequencies listed here (in bold) belong to the CO stretch in the acyl group. The values are significantly different for the agostic and dihapto forms, with almost perfect agreement between the theoretical value for the dihapto form and the experimental value for the stable intermediate. This result strongly supports the earlier experimental findings that the dihapto form, **d**, is the stable intermediate in noncoordinating solvents during the photodecarbonylation of $Mn(CO)_5COCH_3$. Note also that the positions *and relative intensities* of the other CO stretches (for **d**) agree well with experiment.

One area of disagreement between the current work and the previous interpretation of the experimental work on the decarbonylation reaction is the nature of the intermediate in coordinating solvents such as THF. Although Boese et al. observed essentially no difference in the frequency of the acyl CO stretch for the intermediate in methylcyclohexane (1607 cm^{-1}) and THF (1602 cm^{-1}) they assigned (on the basis of reactivity considerations) the structure of the intermediate in THF as a species with explicit solvent coordination and a η^1 acyl group, i.e., $Mn(THF)(CO)_4(\eta^1\text{-}COCH_3)$. We have calculated the carbonyl stretching frequencies of two different conformations of this solvated species (Figure 7) and find values of 1661 and 1677 cm^{-1} for the acyl CO stretch. These values compare very well with the experimental value[18,19] for $Mn(CO)_5(COCH_3)$ (1661 cm^{-1}) and clearly demonstrate that a significant change in the acyl CO stretching frequency would be expected if the acyl bonding mode shifted from η^2 to η^1 due to solvent coordination. In addition, the relative intensities of the other CO stretches are inconsistent with experiment for **f** and **g**. These structures have high-intensity absorptions centered around 1950 cm^{-1} and a lower intensity absorption about 20 cm^{-1} higher. The experimental spectra show just the opposite trend. In summary, our calculations are consistent with the intermediate in the photodecarbonylation reaction being unsolvated **d**, even in THF.[37]

(37) In fact, in their first paper (ref 18) Boese and Ford argued that the similarity of the CO frequencies in methylcyclohexane and THF implied that the dihapto form existed in both solvents. Only in their second paper did they use reactivity arguments to conclude that coordinating solvents explicitly solvated the intermediate.

Conclusions

There are at least two reaction channels for the nonsolvent assisted thermal carbonylation of pentacarbonyl(methyl)manganese(I). Both channels follow a multistep mechanism. The first channel goes through an about 15 kcal/mol activation barrier in its first step which can be characterized as methyl migration. The agostically stabilized intermediate is then attacked by the incoming CO from the acyl carbon side, and forms the overall product. The effective activation energy of the first channel was found to be about 20 kcal/mol at the B3LYP level, in excellent agreement with experimental data extrapolated for solvent effects. In the second channel, the agostic intermediate **e** proceeds to the dihapto species **d**, which is then attacked by CO on the O side. Neither of the intermediates contain the acyl group in the traditional conformation. The ideal bond angles are significantly distorted by the β-agostic interaction or by the η^2 bonding through the acyl oxygen atom. In fact, the traditional η^1-acyl conformation is a transition state (**ts2**) in this system and represents the highest energy stationary point on the potential energy surface. It was shown that the instability of this species is a consequence of the nature of the LUMO, which is ideally suited for internal nucleophilic attack from both the carbon and oxygen side of the acyl group.

Given reasonable assumptions concerning the preexponential factors for bi- and unimolecular reactions, it was demonstrated that only channel 1 yields a rate law consistent with experiment.

Analysis of vibrational frequencies of the agostic and dihapto species supports the experimental observation that the photodecarbonylation proceeds along the second channel, with the dihapto species being the long-lived intermediate. Consequently, these two processes are not the forward and reverse process of the same chemical reaction. Furthermore, there is no computational evidence that the dihapto species generated in the photodecarbonylation of $Mn(CO)_5(COCH_3)$ is explicitly solvated, even in coordinating solvents such as THF.

Acknowledgment. This work was supported by the Robert A. Welch Foundation (grant Y-0743) and the National Science Foundation. The authors also thank Ted O'Brian for his contribution to the early stages of this project, as well as Dr. Simon W. North at Texas A&M for valuable discussions on reaction kinetics and Professor F. A. Cotton for helpful comments. We thank the Swiss Center of Supercomputing for CPU time on the NEC-SX4.

Supporting Information Available: Cartesian coordinates and energies for all stationary points (PDF). This material is available free of charge via the Internet at http://pubs.acs.org.

JA993441V